nature communications

Article

https://doi.org/10.1038/s41467-024-54920-9

The dysadherin/MMP9 axis modifies the extracellular matrix to accelerate colorectal cancer progression

Received: 12 February 2024

Accepted: 26 November 2024

Published online: 30 November 2024

Check for updates

Choong-Jae Lee, Tae-Young Jang, So-El Jeon, Hyeon-Ji Yun, Yeong-Hoon Cho, Da-Ye Lim & Jeong-Seok Nam

The dynamic alteration of the tumor microenvironment (TME) serves as a driving force behind the progression and metastasis of colorectal cancer (CRC). Within the intricate TME, a pivotal player is the extracellular matrix (ECM), where modifications in components, degradation, and stiffness are considered critical factors in tumor development. In this study, we find that the membrane glycoprotein dysadherin directly targets matrix metalloprotease 9 (MMP9), initiating ECM remodeling within the TME and amplifying cancer progression. Mechanistically, the dysadherin/MMP9 axis not only enhances CRC cell invasiveness and ECM proteolytic activity but also activates cancer-associated fibroblasts, orchestrating the restructuring of the ECM through the synthesis of its components in human CRC cells, patient samples, and mouse models. Notably, disruption of ECM reorganization by dysadherin knockout results in a discernible reduction in the immunosuppressive and proangiogenic milieu in a humanized mouse model. Intriguingly, these effects are reversed upon the overexpression of MMP9, highlighting the intricate and pivotal role of the dysadherin/MMP9 axis in shaping the development of a malignant TME. Therefore, our findings not only highlight that dysadherin contributes to CRC progression by influencing the TME through ECM remodeling but also suggest that dysadherin may be a potential therapeutic target for CRC.

Colorectal cancer (CRC) is a prevalent and widespread cancer, and metastasis is the leading cause of CRC mortality[1–3]. The process of CRC progression and metastasis is influenced not only by somatic mutations in tumor suppressor genes or oncogenes but also by the rearrangement of tumor microenvironment (TME) components[4,5]. The TME consists of cellular components, including fibroblasts, endothelial cells, and immune cells, and noncellular components[6,7]. Communication between neoplastic cells and adjacent stromal cells begins at the earliest stage of tumor formation and continues during primary growth, local invasion, and metastasis via immune escape, neovascularization, and the acquisition of a malignant phenotype[8,9]. In addition, tumor progression is dependent on noncellular components, which include bioactive agents as well as mechanical properties[10,11]. The extensive interactions among tumor cells and the TME have complicated efforts to understand the tumor development process. Therefore, further comprehensive analyses of the interaction between CRC cells and the TME are imperative.

The extracellular matrix (ECM) is a key noncellular component of the TME and is produced by different types of cells to provide biophysical and biochemical support. During tumor progression, the ECM undergoes a persistent remodeling process characterized by ECM component deposition, modification, and degradation. In the early stage, tumor cell-derived growth factors and inflammatory factors recruit and activate stromal cells, leading to the secretion and

School of Life Sciences, Gwangju Institute of Science and Technology, Gwangju 61005, Republic of Korea. e-mail: namje@gist.ac.kr

deposition of ECM components[12–16]. Moreover, ECM-modifying enzymes such as lysyl oxidases and prolyl-4-hydroxylases are expressed by tumor cells and stromal cells and cross-link and align with the ECM, increasing matrix stiffness around tumors[17,18]. Both ECM deposition and stiffness increase the ability of tumors to evade immune surveillance and trigger mechanosignaling mediated by integrins[19]. During tumor cell migration and invasion, ECM degradation by proteolytic enzymes or force-mediated ECM breakage could make a path for tumor cells to attain proliferative, invasive, and migratory features. At premetastatic sites, tumor cell-derived factors such as growth factors and cytokines activate cancer-associated fibroblasts (CAFs) to remodel the ECM and interact with other stromal cells, such as endothelial cells and immune cells, thereby forming a favorable microenvironment and promoting the colonization of metastatic tumor cells[19,20]. Notably, the remodeling of the ECM and subsequent changes in biomechanical properties affect various cellular functions, including the proliferation, migration, and invasion of cancer cells, as well as premetastatic TME formation[21]. Thus, there have been an increasing number of studies that have focused on the effects of ECM remodeling on tumor progression and metastasis.

Dysadherin is a tumor-associated cell membrane glycoprotein with an FXYD motif whose expression is significantly correlated with the aggressive phenotype of cancer[22]. Clinical studies have shown that high dysadherin expression in tumors is correlated with clinicopathological features such as distant metastasis, recurrence, and poor prognosis[23–25]. Similarly, dysadherin promotes metastatic potential by regulating cytoskeletal rearrangement and cell–cell adhesion[26,27]. A recent study revealed that dysadherin facilitates cancer cell adhesion to fibronectin and thereby generates mechanical forces in cells via stiffness and activates integrin/FAK signaling in mechanotransduction[24]. Integrin signaling in cancer cells contributes to cancer progression by regulating both intratumoral signaling pathways and the TME through diverse growth factors and cytokines[28–30]. In addition, ECM stiffening affects the recruitment and activation of protumorigenic immune cells, such as those that inhibit T-cell activity and M2 polarization of macrophages, thereby promoting inflammation and metastasis[31–34]. Taken together, these findings suggest that dysadherin may play a pivotal role in modulating the TME. Therefore, in-depth research on dysadherin can reveal profound interactions between cancer cells and the TME.

In this work, we elucidate the role of dysadherin in controlling ECM dynamics, which contributes to CRC metastatic progression. We confirm that dysadherin upregulates matrix metalloprotease 9 (MMP9) expression and increases ECM degradation to increase the invasive and metastatic potential of CRC cells. In addition, the dysadherin/MMP9 axis activates CAFs to promote ECM deposition and the formation of a malignant TME, contributing to tumor progression. These findings provide mechanistic insight into dysadherin, potentially leading to promising opportunities for therapeutic strategies targeting CRC.

Results

Dysadherin expression is linked to ECM remodeling in CRC

We performed a gene set enrichment analysis (GSEA) of the gene expression profiles of CRC patients (GSE21510). ECM remodeling-related signatures, such as collagen degradation and formation, MMP expression, and ECM degradation were upregulated in tumor tissue compared to normal tissue (Fig. 1a). In addition, we analyzed the single-cell RNA sequencing (scRNA-seq) data of CRC patients (GSE144735). We clustered the cells according to cell type (Supplementary Fig. 1a). After grouping the normal and tumor cells in to the epithelial cluster, the genes identified as differentially expressed genes (DEGs) between the tumor cells and normal cells were subjected to pathway analysis. The gene signatures related to ECM alteration and modification was significantly upregulated in tumor cells (Fig. 1b). Trajectory analysis of the tumor cell cluster from GSE144735 revealed that the expression of ECM remodeling-related genes and *dysadherin* (*FXYD5*) was increased in advanced cancer cells, with a potential positive correlation (Supplementary Fig. 1b). Network analysis revealed that ECM remodeling was associated with dysadherin (Supplementary Fig. 1c). Consistent with these findings, we assessed dysadherin expression and ECM remodeling via the expression of ECM components and proteolytic activity in CRC patient tissues (Supplementary Data 1, Table S1). The expression of collagen I, fibronectin and dysadherin was upregulated in CRC tissue, whereas the expression of laminin and collagen IV was downregulated, and the increased fluorescence intensity of quenched fluorogenic DQ-collagen I and DQ-gelatin indicated proteolytic activity in CRC tissue (Fig. 1c, Supplementary Fig. 2a, b). Furthermore, dysadherin expression and ECM remodeling increased with the advancing of CRC progression (Supplementary Fig. 2b).

To investigate the role of dysadherin in CRC, we confirmed its elevated expression in cancer (GSE21510) and compared the gene expression profiles of cancers by dividing 104 CRC patient samples into high and low *dysadherin* expression groups based on the median expression value (Fig. 1d, Supplementary Fig. 3a). Using DEGs in cancers with high *dysadherin* expression, we performed GSEA. As a result, the ECM remodeling-related signature, along with ECM degradation, ECM organization and collagen formation, was significantly enriched in these cancers (Fig. 1d). Furthermore, we analyzed the scRNA-seq data of CRC patients (GSE225857). We again clustered cells according to cell type (Supplementary Fig. 3b). Next, to verify the effect of *dysadherin* expression on tumor cells, we grouped dysadherin-expressing and -nonexpressing tumor cells. After grouping the cells according to *dysadherin* expression, we performed pathway analysis of the DEGs between groups and found that tumor cells with *dysadherin* expression had upregulated ECM remodeling-related gene signatures such as organization and degradation of ECM, collagen formation and degradation (Fig. 1e). Consistent with these findings, we assessed the ECM remodeling potential of dysadherin-knockout ($Fxyd5^{-/-}$) mice, which were generated in a previous study. There were significantly fewer tumors in $Fxyd5^{-/-}$ mice than wild-type mice (Supplementary Fig. 3c). Approximately 11.2% of tumors from $Apc^{Min/+}$;$Fxyd5^{+/+}$ mice exhibited local invasion through a fissure in the mucosal muscle layer; however, all tumors from $Apc^{Min/+}$;$Fxyd5^{-/-}$ mice exhibited a noninvasive phenotype (Supplementary Fig. 3d). The invasive fronts of tumors from $Apc^{Min/+}$;$Fxyd5^{+/+}$ mice showed greater collagen I deposition and ECM proteolytic activity than did those from $Apc^{Min/+}$;$Fxyd5^{-/-}$ mice (Fig. 1f). Interestingly, *Fxyd5* depletion did not affect collagen I deposition and ECM proteolytic activity in the normal intestinal tissues (Supplementary Fig. 3e). In 3D culture, upon establishing tumoroids, *Fxyd5* depletion also reduced proteolytic activity (Fig. 1g). Taken together, these results suggest that dysadherin plays an important role in ECM remodeling in CRC cells.

Dysadherin modulates MMP9 expression by activating the FAK/c-JUN axis

To obtain further mechanistic insight, we conducted ingenuity pathway analysis (IPA) and GSEA of RNA-seq data from dysadherin knockout (KO) SW480 cells[24]. Intriguingly, IPA revealed the potential involvement of dysadherin in TME pathways (Supplementary Fig. 4a). The expression of genes involved in collagen degradation, collagen formation, and MMP activation was significantly greater in the wild-type SW480 cells than in the dysadherin KO SW480 cells (Fig. 2a). When the genes associated with collagen degradation, collagen formation, and activation of MMP were compared, three genes were found to be common, and the expression of *MMP9* was most significantly downregulated in dysadherin KO SW480 cells (Fig. 2b). In a previous study, we revealed that dysadherin regulates tumor progression and malignancy through integrin-FAK signaling[24]; therefore,

https://doi.org/10.1038/s41467-024-54920-9

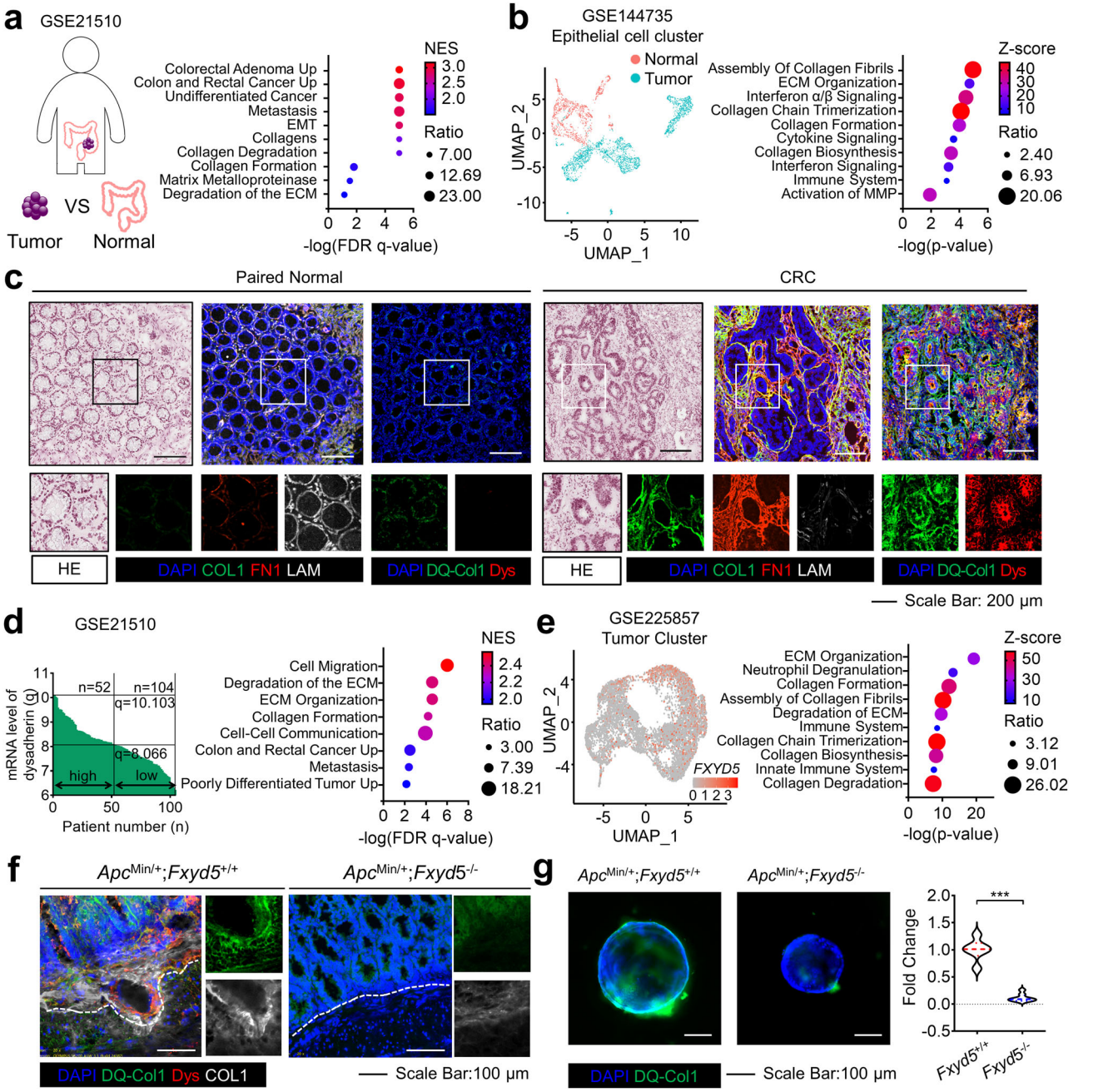

Fig. 1 | Dysadherin expression is associated with ECM remodeling in CRC. a The list of DEGs in tumor tissue ($n = 52$) compared to normal tissue ($n = 25$) obtained from the Gene Expression Omnibus (GEO) database (GSE21510) was obtained through R2 analyses with the GEO platform ($p < 0.001$) and used for GSEA to determine the associated gene signatures. BioRender software (https://www.biorender.com/) was used to create the figure under an academic license. **b** UMAP plot of the epithelial cell cluster of CRC patients from GSE144735 and GSEA of genes differentially expressed between tumors (n = 2212) and normal ($n = 1144$) cells. **c** In situ zymography analysis and IF analysis of ECM components and dysadherin expression in CRC patient tissue ($n = 50$). **d** Left: Dysadherin expression in patients with CRC. mRNA expression data from patient tumors were obtained from the GEO database (GSE21510), and patients were divided into two groups according to the median dysadherin expression level (dysadherin^{high}, $n = 52$; dysadherin^{low}, $n = 52$). Right: GSEA of DEGs between the dysadherin^{high} and dysadherin^{low} cohorts. **e** Left: UMAP plot of the tumor cell cluster of CRC patients from GSE225857, colored according to dysadherin (FXYD5) expression (FXYD5^{Pos}, $n = 1535$; FXYD5^{Neg}, $n = 6486$). Right: GSEA of genes differentially expressed between dysadherin-expressing cells and dysadherin-nonexpressing cells. **f** In situ zymography and IF of the intestines of 24-week-old *Apc*$^{Min/+}$ mice with or without dysadherin (*Fxyd5*) knockout labeled for DQ-collagen I, dysadherin, and collagen I ($n = 5$ mice per group). **g** In situ zymography analysis of mouse intestinal tumor organoids ($n = 10$/group). IF intensity data are presented as means ± SEMs. *** indicates $p < 0.001$. Statistical significance was determined by unpaired two-tailed Student's t tests for comparisons between two groups. Source data are provided as a Source Data file. Dys dysadherin, Col1 collagen I, FN1 fibronectin, LAM laminin, DQ-Col1 DQCollagen I, NES normalized enrichment score, FDR false discovery rate, HE hematoxylin and eosin staining.

we investigated that the dysadherin/FAK axis regulates ECM remodeling, tumor malignancy, and metastasis through controlling the expression of MMP9 by IPA (Fig. 2c). Analysis of CRC patient tissue (Supplementary Data 1, 2 confirmed that the expression of dysadherin and MMP9 was greater in tumor tissue than in paired normal tissue and that dysadherin and MMP9 were positively correlated (Supplementary Fig. 4b–e). A correlation between dysadherin and MMP9 was also confirmed by analyzing the GSE73255 dataset (Supplementary Fig. 4f).

https://doi.org/10.1038/s41467-024-54920-9

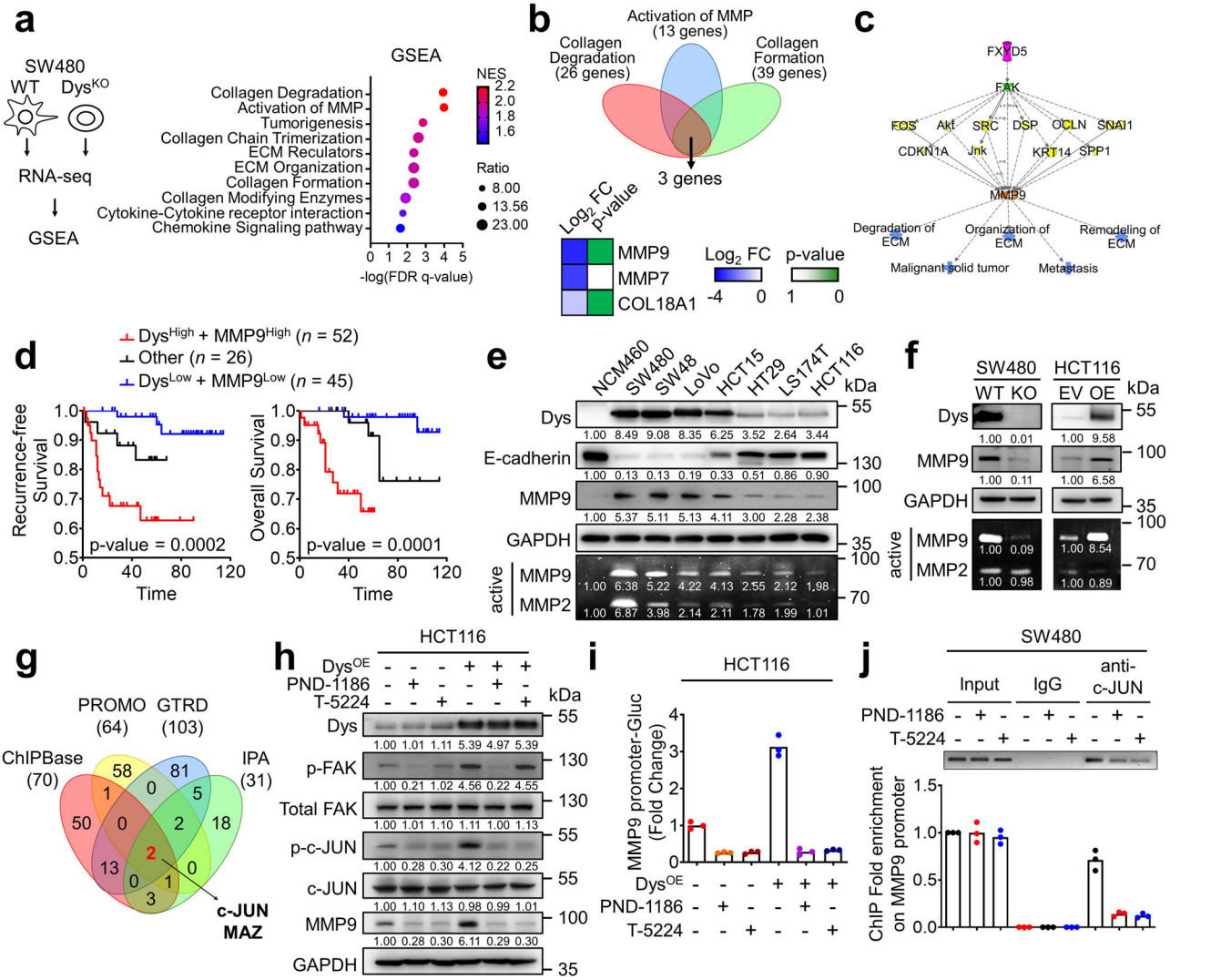

Fig. 2 | Dysadherin enhances MMP9 expression via the FAK/c-JUN axis. a GSEA was performed using the mRNA-sequencing profiles of dysadherin KO and WT SW480 cells, which was performed in previous study[24]. **b** Three candidate genes related to three gene signatures were identified. Heatmap indicated FC and p-value (unpaired two-tailed Student's *t* tests) from mRNA-sequencing data. **c** Downstream analysis indicating the potential link between dysadherin/FAK pathway and MMP9, leading to ECM remodeling, malignancy, and metastasis. **d** Kaplan-Meier analysis of CRC patients by dividing into three groups according to dysadherin and MMP9 expression. Statistical significance was determined by log-rank tests. **e** Immunoblotting for dysadherin, E-cadherin, and MMP9 expression and gel zymography in human CRC and normal colon cell lines. **f** Immunoblotting for dysadherin and MMP9 and gel zymography in dysadherin KO or OE CRC cells. **g** Venn diagram showing overlapping transcription factors that are positively correlated with MMP9 expression. **h** Immunoblotting for p-FAK, total FAK, p-c-JUN, total c-JUN, and MMP9 in EV and dysadherin OE HCT116 cells treated with or without 1 μM PND-1186 or 20 μM T-5224. **i** Promoter activity of MMP9 was tested via luciferase reporter assay. MMP9 promoter region-containing vector was transfected into EV and dysadherin OE HCT116 cells, and cells were treated with or without PND-1186 or T-5224. Total transcription was normalized to β-galactosidase transcription and is presented as fold change with respect to nontreated HCT116 cells. **j** Binding affinity of c-JUN on MMP9 promoter with or without PND-1186 or T-5224 in SW480 cells was tested via ChIP assay. **i, j** $n = 3$ biological replicates, representative of three independent experiments with similar results. Immunoblot assays were independently repeated three times with similar results. The data are presented as the means ± SEMs. *, **, and *** indicate $p < 0.05$, $p < 0.01$ and $p < 0.001$, respectively. Statistical significance was determined by one-way ANOVA with Dunnett's multiple comparison test for comparisons among three groups. Source data are provided as a Source Data file. FC fold change, P paired normal, T tumor, WT wild-type, KO knockout, EV empty vector, OE overexpression, Ct threshold of cycle, dCt delta Ct, difference of Ct value between target and housekeeping gene.

Moreover, immunofluorescence (IF) analysis revealed that CRC patients (Supplementary Data 2) with high dysadherin- or MMP9-expressing tumors had significantly shorter overall survival (OS) and recurrence-free survival (RFS) (Supplementary Fig. 4g). Analysis by combining two genes revealed that patients with high expression of both genes had worse OS and RFS than other patients (Fig. 2d). These data were supported by survival analysis of the GSE14333/GSE17538 dataset (Supplementary Fig. 4h). In addition, dysadherin and MMP9 were expressed in CRC cell lines but not in a normal colon cell line (NCM460D), and there was a positive correlation between dysadherin expression and MMP9 expression and activity (Fig. 2e, Supplementary Fig. 5a). When dysadherin expression was depleted, the expression and activity of MMP9 decreased. Conversely, dysadherin overexpression (OE) significantly enhanced the expression and activity of MMP9 (Fig. 2f, Supplementary Fig. 5b). Dysadherin knockdown (KD) by siRNA downregulated MMP9 expression and activation in patient-derived primary cells (Table S2) and in SNU-254 human rectal cancer cells (Supplementary Fig. 5c, d). Incidentally, the activity of MMP2 was elevated in CRC cells and positively correlated with that of MMP9[35] (Fig. 2e, Supplementary Fig. 5a), but remained unaffected by

dysadherin manipulation (Fig. 2f, Supplementary Fig. 5b–d). Moreover, dysadherin KD decreased MMP9 expression in MDA-MB-231 human breast cancer cells, and dysadherin OE increased MMP9 expression in PLC/PRF/5 human liver cancer cells (Supplementary Fig. 5e). Thus, dysadherin expression regulated MMP9 expression in various types of cancer.

To obtain additional mechanistic insight, we used four programs (ChipBase, PROMO, GTRD, and IPA) to identify c-JUN and MAZ as candidate transcription factors of MMP9 (Fig. 2g). We chose a c-JUN as the mediator of MMP9 transcriptional activation via gene KD assay (Supplementary Fig. 5f). FAK regulates the transcriptional activity of c-JUN[36]. Dysadherin activates the ECM-integrin pathway, leading to FAK activation[24]. An inhibitory peptide was developed to block this effect on cancer cell growth[24]. IF staining validated that the peptide reduced the integrin activation and p-FAK expression (Supplementary Fig. 5g). Immunoblot assay confirmed that the integrin inhibitor MK-0429 decreased the dysadherin OE-induced p-FAK expression (Supplementary Fig. 5h). Next, to verify that the integrin/FAK axis regulates MMP9 expression via c-JUN, we performed immunoblot and luciferase reporter assays using MK-0429, the FAK inhibitor PND-1186 and the c-JUN inhibitor T-5224. Dysadherin OE increased the expression of p-c-JUN and MMP9, which was reduced by treatment with these inhibitors (Fig. 2h, Supplementary Fig. 5h). Similarly, dysadherin OE increased luciferase activity, but this increase was reversed after treatment with these inhibitors (Fig. 2i, Supplementary Fig. 5i). By performing a chromatin immunoprecipitation (ChIP) assay, we confirmed that c-JUN directly bound to the promoter region of MMP9 and that PND-1186 and T-5224 reduced the binding affinity (Fig. 2j). Therefore, our results suggest that dysadherin transcriptionally activates MMP9 expression via the integrin/FAK/c-JUN axis.

The dysadherin/MMP9 axis promotes ECM deposition and CRC metastasis through CAF activation

To validate the role of dysadherin/MMP9 in CRC metastatic progression in vivo, we selected the most effective siRNA sequence targeting MMP9 and then constructed the inducible shRNA vector for establishing inducible MMP9 KD cell lines using dysadherin OE HCT116 cells (Supplementary Fig. 6a, b). We performed an intrasplenic xenograft experiment in NOD.Cg-Prkdc^{scid} Il2rg^{tm1Wjl}/SzJ (NSG) mice. Dysadherin OE significantly enhanced the expression of MMP9 and the colonization potential of CRC cells in the liver, and these changes were reversed by doxycycline-induced KD of MMP9. Following doxycycline removal, MMP9 expression and colonization potential were restored (Fig. 3a, Supplementary Fig. 6c). Next, dysadherin OE increased proteolytic activity and collagen I deposition in the liver, but these effects decreased upon induction of MMP9 KD by doxycycline. When doxycycline treatment was withdrawn, proteolytic activity and collagen I deposition increased again (Fig. 3b, Supplementary Fig. 6d). During metastatic progression, ECM reorganization is conducted mainly by CAFs, which can synthesize ECM components when activated. To investigate the correlation between dysadherin expression in cancer cells and that in CAFs, we conducted spatial transcriptomic analysis. Through the expression pattern of EPCAM, we distinguished cancer tissue from stromal tissue (Supplementary Fig. 7a). There were more active CAFs, represented by increased α-smooth muscle actin (α-SMA) expression, surrounding high dysadherin-expressing cancer cells compared to low dysadherin-expressing cells (Fig. 3c). Similarly, in metastatic tumors in the mouse liver, dysadherin OE increased the α-SMA expression, but these changes reversed upon MMP9 KD. When MMP9 expression was restored, they upregulated again (Fig. 3d, Supplementary Fig. 7b). Of note, CAF activation was consistently observed in lesions with ECM remodeling (Supplementary Fig. 7c). We also confirmed the role of dysadherin in regulating CAF activation in intestinal tumors from *Apc*$^{Min/+}$;*Fxyd5*$^{+/+}$ mice and *Apc*$^{Min/+}$;*Fxyd5*$^{-/-}$ mice, which exhibited a striking reduction in CAF activation in the absence of dysadherin (Supplementary Fig. 8a). Next, we verified that the ECM remodeling and CAF activation were elevated in malignant tumors. ECM proteolytic activity and CAF activation were greater in metastatic CRC patients compared with nonmetastatic CRC patients (Fig. 3e, Supplementary Fig. 8b, Supplementary Data 1). The expression of dysadherin, MMP9, and collagen I was upregulated in patients with metastatic CRC (Supplementary Fig. 8c). In summary, high dysadherin-expressing cancer cells exhibited malignant characteristics and a high potential to activate CAFs. Therefore, our results indicate that the dysadherin/MMP9 axis promotes ECM proteolysis and CAF activation, contributing to metastatic progression.

Dysadherin expression enhances ECM proteolysis and invasive potential of CRC cells

We verified the role of dysadherin/MMP9 in ECM degradation and cell invasion in vitro. Dysadherin OE increased ECM proteolytic activity and cell invasiveness, but these effects were reduced upon doxycycline-induced MMP9 KD. MMP9 expression was restored following doxycycline withdrawal, and the cells exhibited normalization of ECM proteolytic activity and cell invasiveness (Fig. 4a, b). Next, the results of an anchorage-independent growth assay showed that dysadherin OE increased the number of colonies but that MMP9 KD decreased the number of colonies (Fig. 4c). These results suggest that the proteolytic activity of MMP9 cleaves cell surface proteins such as cytokine receptors and cell adhesion molecules, promoting invasion and metastasis as well as regulating signaling pathways that control cell growth and survival[37–39]. In addition, we established MMP9 OE cell lines using dysadherin KO SW480 cells (Supplementary Fig. 9a). MMP9 OE increased proteolytic activity in the ECM and the number of invading cells, and decreased the number of colonies which were reduced by dysadherin KO (Supplementary Fig. 9b–d).

Several studies have reported that MMP9 activates latent transforming growth factor β (TGF-β) to its active form, which activates CAFs, contributing to modulating the TME via the secretion of ECM components, ECM-modifying enzymes, and tumor-promoting factors[40]. First, through enzyme-linked immunosorbent assay (ELISA), we verified that the dysadherin/MMP9 axis activated TGF-β in cancer cells. Dysadherin OE resulted in an increase in active TGF-β level, which was subsequently reversed upon MMP9 KD. The removal of doxycycline led to the restoration of active TGF-β levels (Supplementary Fig. 10a), which was supported by a decrease in TGF-β activation via an MMP9 inhibitor (Supplementary Fig. 10b). In addition, dysadherin KO downregulated active TGF-β, but this effect was reversed upon MMP9 OE (Supplementary Fig. 10c). We also assessed the expression of ECM molecules, ECM-modifying enzymes, and tumor-promoting factors in MRC-5 cells, a human normal fibroblast line, treated with conditioned media (CM) from CRC cell lines. The levels of these markers were significantly increased in MRC-5 cells treated with CM from dysadherin OE HCT116 cells. The expression of these genes decreased when MRC-5 cells were cultured with CM from doxycycline-induced MMP9 KD in dysadherin OE HCT116 cells, but these effects were reversed upon doxycycline withdrawal (Fig. 4d). When MRC-5 cells were cultured with CM from dysadherin KO SW480 cells, there was low expression of markers, and these changes were reversed when the cells were treated with CM from MMP9 OE/dysadherin KO SW480 cells (Supplementary Fig. 10d). Furthermore, we assessed the protein levels of CAF markers, collagen I and p-SMAD2/3 in CAFs activated by the dysadherin/MMP9 axis. The levels of CAF markers, collagen I and p-SMAD2/3 significantly increased in MRC-5 cells treated with CM from dysadherin OE HCT116 cells. The expression of them decreased when MRC-5 cells were cultured with CM from doxycycline-treated dysadherin OE HCT116 cells, but these effects were restored upon doxycycline withdrawal (Fig. 4e, f). When cultured with CM from dysadherin KO SW480 cells, MRC-5 cells had low expression of CAF markers, collagen I and p-SMAD2/3, and these

https://doi.org/10.1038/s41467-024-54920-9

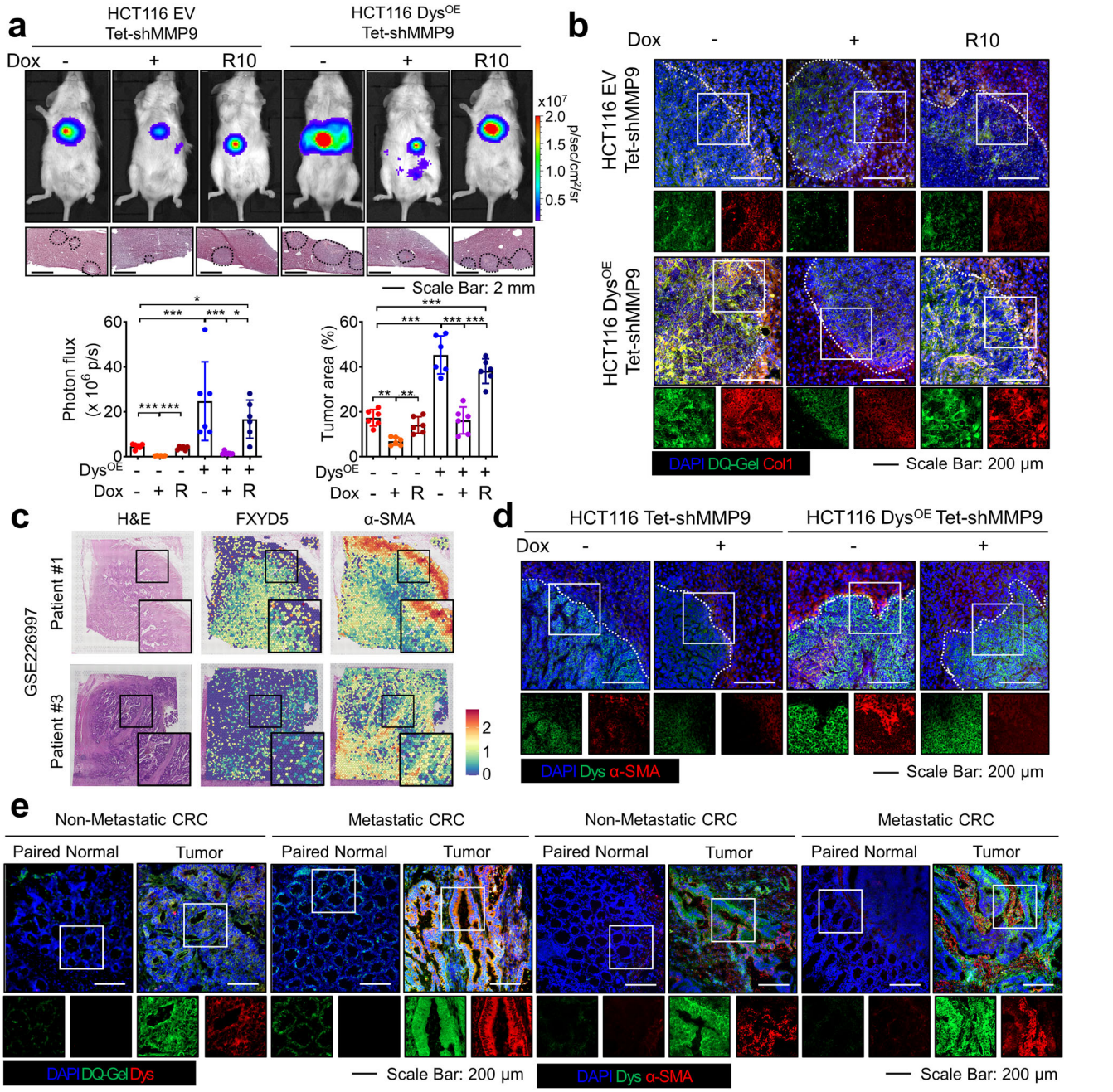

Fig. 3 | The dysadherin/MMP9 axis enhances the metastatic potential via CAF activation. a Top: Representative in vivo bioluminescence images of mice (n = 6/group) injected with luciferase-labeled HCT116 cells transfected with EV or dysadherin OE vectors along with Tet-shMMP9. Bottom: the corresponding graph shows the results of the quantitative analysis of the region of interest. Middle: Representative hematoxylin and eosin-stained livers with metastasis. R means 'rescued following doxycycline withdrawal' **b** IF analysis of collagen I and in situ zymography analysis of mouse livers with metastatic tumors ($n = 6$/group). **c** Spatial plots showing the spatial expression pattern of α-SMA, a CAF marker, and dysadherin (FXYD5) using GSE226997 dataset. **d** IF analysis of dysadherin and α-SMA in mouse livers with metastatic tumors ($n = 6$/group). **e** In situ zymography analysis and IF analysis of dysadherin and α-SMA expression in CRC patient tissue (Non-metastatic CRC, $n = 36$; Metastatic CRC, $n = 14$). The data in **a** are presented as means ± SEMs. *, **, and *** indicate $p < 0.05$, $p < 0.01$ and $p < 0.001$, respectively. Statistical significance was determined by one-way ANOVA with Dunnett's multiple comparison test for comparisons among more than three groups. Source data are provided as a Source Data file.

changes were reversed when the cells were treated with CM from MMP9 OE/dysadherin KO SW480 cells (Supplementary Fig. 10e). Of note, TGF-β inhibitors, LY-364947 and 1D11 decreased dysadherin-mediated CAF activation (Supplementary Fig. 10f), whereas TGF-β ligand had the opposite effect (Supplementary Fig. 10g). Taken together, these findings indicate that the dysadherin/MMP9 axis activates CAFs via TGF-β activation and that activated CAFs secrete various factors which facilitate ECM reorganization and modification and promote tumor progression.

ECM remodeling by the dysadherin/MMP9 axis induces a premetastatic TME

Several studies have shown that ECM dynamics facilitate interactions with cancer cells and stromal cells, leading to premetastatic niche formation[19,31]. In particular, ECM remodeling shifts the TME from an immunoinflammatory tumor, i.e., a hot tumor, to an immune-excluded tumor, i.e., a cold tumor, concurrently establishing a proangiogenic milieu[31]. To verify the role of dysadherin/MMP9 axis-mediated ECM dynamics in TME alteration, we established a humanized mouse model

https://doi.org/10.1038/s41467-024-54920-9

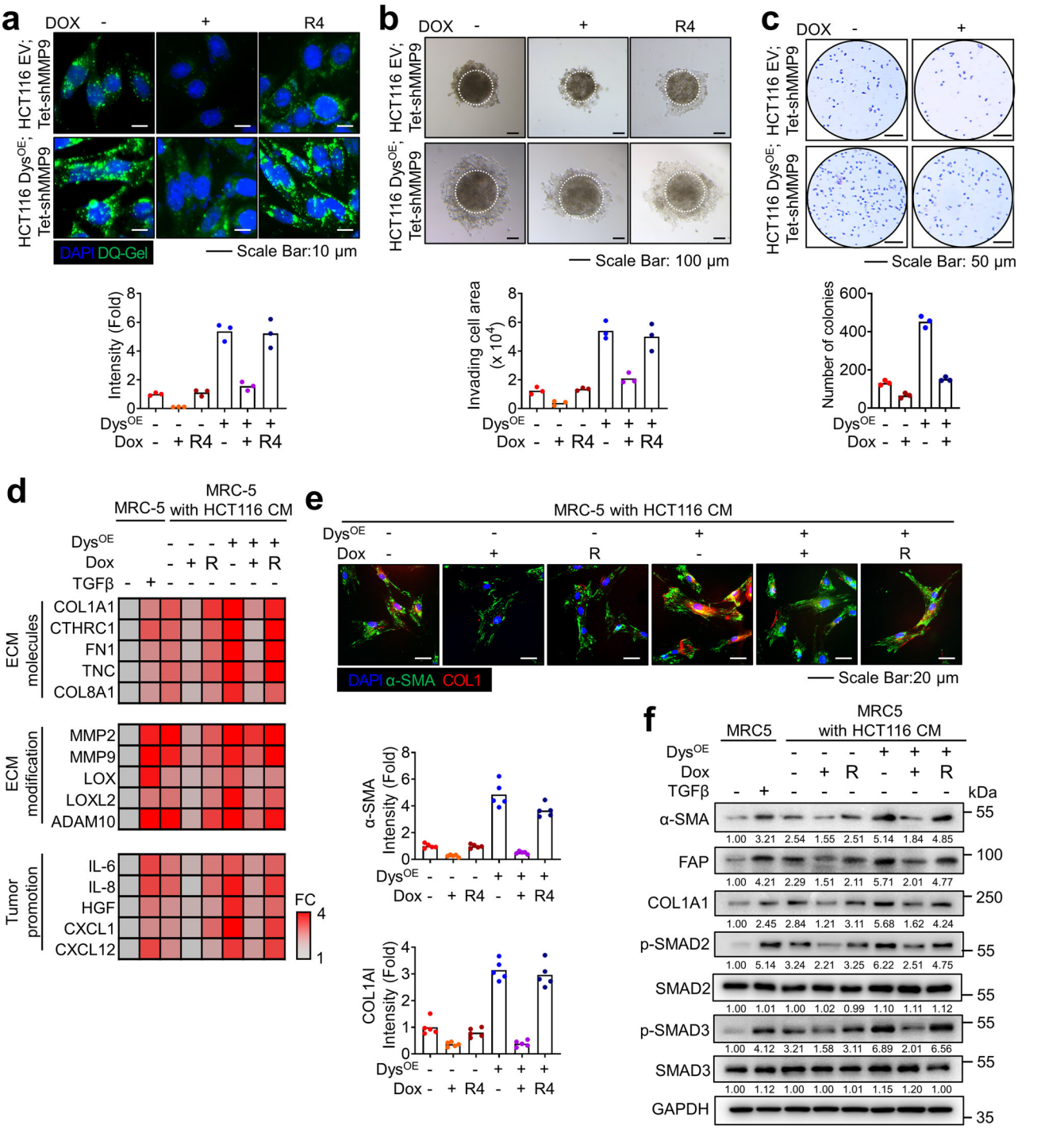

Fig. 4 | The dysadherin/MMP9 axis increases proteolytic activity, invasive potential and CAF activation in the ECM. In situ zymography analysis (**a**), 3D invasion assay (**b**), and anchorage-independent growth assay (**c**) of Tet-pLKO-shMMP9 transfected EV and dysadherin OE HCT116 cells with or without doxycycline ($n = 3$ biological replicates, representative of three independent experiments with similar results). **d** Heatmap comparing the relative expression of factors related to collagens, ECM modification, and tumor promotion in MRC-5 cells cultured with culture medium (CM) from control or dysadherin OE HCT116 cells transfected with Tet-shMMP9 ($n = 3$ biological replicates). **e** IF analysis of α-SMA and collagen I expression in MRC-5 cells cultured with CM. The corresponding quantitation of 5 replicates is shown below ($n = 5$ biological replicates, representative of three independent experiments with similar results). **f** Immunoblot analyses of the expression of the α-SMA and fibroblast activation protein (FAP) as CAF markers, collagen I, p-SMAD2/3 and total SMAD2/3 in MRC-5 cells cultured with CM. Immunoblot assay was independently repeated three times with similar results. The data are presented as means ± SEMs. *, **, and *** indicate $p < 0.05$, $p < 0.01$ and $p < 0.001$, respectively. Statistical significance was determined by one-way ANOVA with Dunnett's multiple comparison test for comparisons among six or four groups. Source data are provided as a Source Data file.

(Supplementary Fig. 11a) and performed intrasplenic xenograft experiments using MMP9 OE in dysadherin wild-type and KO SW480 cells. Dysadherin KO significantly reduced the metastatic potential of injected cancer cells, but this effect was reversed upon MMP9 OE (Fig. 5a). First, we explored ECM reorganization and CAF engagement during metastasis. Both ECM remodeling and CAF activation were decreased at metastatic nodules in dysadherin KO cell-injected mice but increased in MMP9 OE cell-injected mice (Fig. 5b, c, Supplementary

https://doi.org/10.1038/s41467-024-54920-9

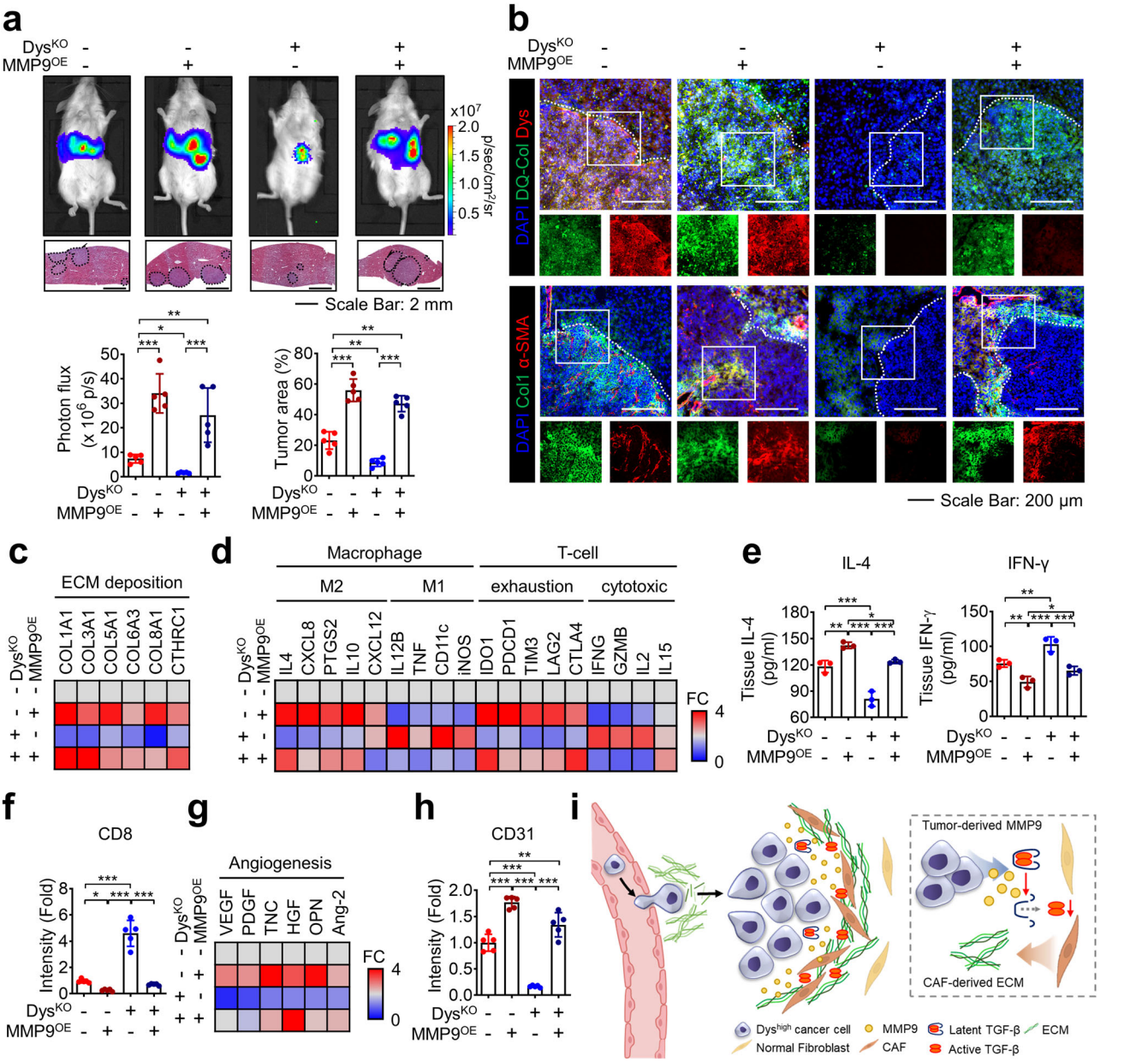

Fig. 5 | The dysadherin/MMP9 axis facilitates metastasis potential by shaping the protumor microenvironment. a Representative in vivo bioluminescence images of mice injected with luciferase-labeled wild-type or dysadherin KO SW480 cells with/without MMP9 OE, accompanied by a corresponding graph showing the quantitative analysis of the region of interest. Middle: Representative hematoxylin and eosin-stained livers with metastasis ($n = 5$/group). **b** In situ zymography analysis and IF analysis of dysadherin, α-SMA, and collagen I expression in mouse liver tissue from metastatic tumors. **c** Heatmap comparing the relative expression of ECM deposition factors in metastatic tumors in the mouse liver ($n = 5$/group). **d** Heatmap comparing the relative expression of macrophage polarization and T-cell related markers in metastatic tumors in the mouse liver ($n = 5$/group). **e** Levels of IL-4 and IFN-γ in metastatic tumors, from ELISA data ($n = 3$/group). **f** Quantitative analysis of CD8 IF data from mouse livers with metastatic tumors ($n = 5$/group). **g** Heatmap comparing the relative expression of angiogenesis-related factors in metastatic tumors in the mouse liver ($n = 5$/group). **h** Quantitative analysis of CD31 IF data from mouse livers with metastatic tumors ($n = 5$/group). **i** Schematic summary of the study findings indicating the potential role of dysadherin in cancer cells in promoting ECM remodeling and CAF activation, which contributes to the formation of a malignant TME. BioRender software was used to create the figure under an academic license. The data are presented as means ± SEMs. *, **, and *** indicate $p < 0.05$, $p < 0.01$ and $p < 0.001$, respectively. Statistical significance was determined by one-way ANOVA with Dunnett's multiple comparison test for comparisons among four groups. Source data are provided as a Source Data file.

Fig. 11b). In metastatic lesions, dysadherin KO decreased active TGF-β levels and p-SMAD2 expression in CAFs, whereas MMP9 OE reversed these changes (Supplementary Fig. 11c, d). Interestingly, CAF activation via TGF-β activation was observed to affect primary tumor growth in the $Apc^{Min/+}$ mouse model; however, Fxyd5 KO decreased tumor growth and CAF activation (Supplementary Fig. 12).

Second, we evaluated the expression of markers related to immunosuppression (T-cell exhaustion and M2 macrophages) and immunostimulation (cytotoxic T-cells and M1 macrophages)[41–43]. The expression of immunosuppression markers was decreased, and the expression of immunostimulatory markers was increased in dysadherin KO mice, whereas these effects were reversed following MMP9 OE (Fig. 5d). Moreover, we further tested the two factors with the greatest changes in expression, interferon-γ (IFN-γ) and interleukin-4 (IL-4), via ELISA (Fig. 5e). We validated the expression of immune cell markers by IF staining of metastatic tumors in the mouse liver.

Dysadherin KO increased CD8⁺ T-cell infiltration and M1 macrophages and decreased T-cell exhaustion and M2 macrophages, whereas MMP9 OE reversed these changes (Fig. 5f, Supplementary Fig. 13a, b). Specifically, we observed that dysadherin OE in CRC cells was associated with immune-related pathways, as indicated by bioinformatics analysis, and led to an increase in the immunosuppressive marker PD-L1[44] (Supplementary Fig. 14a). Finally, we tested the expression of angiogenesis markers. Dysadherin KO decreased the expression of angiogenesis-related markers, but MMP9 OE reversed these changes (Fig. 5g), as supported by IF analysis of CD31 expression (Fig. 5h and Supplementary Fig. 13a), whereas the opposite effects were observed in vivo study with dysadherin OE HCT116 cells (Supplementary Fig. 14b). Our data showed that dysadherin/MMP9 axis-induced ECM remodeling led to immunologically cold tumors and formed a proangiogenic milieu. Overall, the results of our study suggest that dysadherin facilitates ECM remodeling and CAF activation by promoting the expression of MMP9, which contributes to the formation of a premetastatic TME during metastatic progression (Fig. 5i).

Discussion

This study revealed that dysadherin-expressing cells contribute to CRC progression via ECM remodeling within the TME. By analyzing bulk and single-cell genomics studies, we found that high dysadherin-expressing cells were positively linked to ECM remodeling-related gene signatures. Mechanistically, dysadherin up-regulates MMP9 expression via FAK/c-JUN axis. Dysadherin expression in cancer cells can promote cellular invasion through the MMP9-ECM degradation axis. In addition, the dysadherin/MMP9 axis activates CAFs, which secrete ECM components and soluble factors related to ECM modification, tumor promotion, and interaction with stromal cells to increase premetastatic TME formation. Notably, our discovery of the dysadherin/MMP9 axis highlights a extrinsic function of dysadherin in CRC progression, thus broadening the role of dysadherin in shaping the malignant TME. Therefore, our findings represent an important step toward elucidating the functional importance of dysadherin in CRC progression.

During tumor progression, tumor cells undergo molecular and phenotypic changes, contributing to tumor heterogeneity[45]. The acquisition of these alterations can result in the emergence of tumor subclones with varying phenotypic advantages, such as invasion, proliferation, and interaction with the TME[46]. Dysadherin expression is heterogeneous in tumors, and its expression is greater in tumor cells than in normal cells; moreover, its expression increases further in tumor cells with greater malignancy[24,26]. In addition, dysadherin intrinsically promotes tumor malignancy through the enhancement of the epithelial–mesenchymal transition (EMT) and cancer stem cell properties[22,27]. In this study, trajectory analysis confirmed that there was a correlation between increased dysadherin expression and cancer progression (Supplementary Fig. 1b). We also showed that high-dysadherin-expressing cancer cells modulate the TME to escape immunosurveillance and induce angiogenesis (Fig. 5d–h, Supplementary Fig. 13a, b, 14b). Taken together, the findings of our study suggest that the impact of dysadherin on cancer cell invasion and metastasis is complex and involves both cell autonomous properties and interactions with the external cellular milieu.

Tumor cells have to detach, migrate, invade, adapt, and reattach via matrix-degrading enzymes and mechanical processes such as cell adhesion and the generation of forces during tumor progression. These processes are determined by the structural and biochemical properties of the ECM as well as by communication with surrounding CAFs[20,21]. Our spatial transcriptomic analysis revealed that high-dysadherin-expressing cells were positively correlated with CAF activation (Fig. 3c, Supplementary Fig. 3e). Dysadherin expression was notably elevated in tumor cells in the invasive region, thereby promoting CAF activation. In addition, our data also confirmed that CAFs secrete factors related to ECM modification (i.e., degradation and reorganization), tumor promotion, and stromal cell stimulation in a coculture system of cancer cells and fibroblasts. Activated CAFs secrete proteolytic enzymes such as MMPs and ADAM, suggesting their pivotal role as leader cells in facilitating cancer cell migration during invasion through the clearance of the interstitial matrix via a proteolytic remodeling process[11]. We also observed that CAFs produced tumor-promoting factors such as IL-6, IL-8, and HGF, which are known to increase tumor survival and migratory and invasive potential[47–49] (Fig. 4d, Supplementary Fig. 4h). The secretion of factors that recruit or activate stromal cells, such as chemokines, orchestrates a favorable TME for invasion and metastasis. Our findings reveal a notable perspective on tumor cell-mediated CAF activation, underscoring the pivotal role of dysadherin in organizing intricate invasive and metastatic processes.

In this study, we revealed that dysadherin/MMP9 axis-mediated ECM reorganization shaped the malignant TME at metastatic sites. The intrasplenic xenograft model reflects tumor-host interactions in liver metastatic colonization with high rate, providing more consistent and reproducible results[50,51]. Our data showed that the dysadherin/MMP9 axis increased the expression of factors related to forming an immunosuppressive and proangiogenic milieu in a metastatic CRC mouse model (Fig. 5d–h, Supplementary Fig. 13, 14). In particular, we confirmed that dysadherin KO increased CD8⁺ T-cell infiltration and decreased angiogenesis, as indicated by CD31 expression; however, these changes were reversed upon MMP9 OE (Supplementary Fig. 13a). ECM-rich tumors lead to the up-regulation of immunosuppressive factors such as IL-10, CCL18, CCL22, and TGF-β, which act as suppressors of infiltrating CD8⁺ T cells. In addition, the release of matrix-bound growth factors, such as VEGF, by ECM proteolysis promotes angiogenesis[10,11]. Overall, ECM remodeling contributes to the formation of immunologically cold tumors and results in a proangiogenic environment. However, concomitantly, dysadherin may exert an impact on malignant TME formation through alternative pathways. A previous study demonstrated that dysadherin upregulates the expression of CCL2, which facilitates the paracrine effects of endothelial cell recruitment[52]. Furthermore, GSEA and IPA results suggested the potential involvement of dysadherin in cytokine signaling and the TME pathway (Fig. 2a, Supplementary Fig. 4a). Thus, further investigation of the relevance of dysadherin in the TME could reveal the multifaceted role of dysadherin in modulating the TME.

Dysadherin expression is increased in cancer cells via oncogene activation or tumor suppressor loss[22,53], supporting that the Apc mutation boosted dysadherin expression in intestinal tumor (Supplementary Fig. 15a). Bioinformatics analysis revealed that oncogenic events in CRC led to dysadherin upregulation (Supplementary Fig. 15b). This protein is expressed in a limited number of cell types including endothelial cells and lymphocytes within TME[22,23,25]. The expression of dysadherin in these cell types may affect TME dynamics. However, previous study revealed that dysadherin depletion in stromal cells has no effect on murine tumor growth[24]. In cancer cells, dysadherin deletion resulted in reduced metastasis rates in xenograft models[24,52] (Fig. 5a). In-depth research on dysadherin expression could help elucidate the role of dysadherin in CRC development.

Overall, we showed that the dysadherin/MMP9 axis promoted not only ECM degradation but also ECM reorganization via CAF activation, contributing to shaping the malignant TME. Our findings reveal the crucial role of dysadherin in the interaction between tumor cells and the TME during malignant progression and may provide a basis for further development of therapeutic strategies to overcome CRC progression.

Methods

Ethics approval

Prior approval for animal studies was obtained from the Institutional Animal Care and Use Committee (IACUC) of the Gwangju Institute of Science and Technology (GIST, No. GIST2021-065). Analysis of dysadherin, ECM molecules, and α-SMA expression and in situ zymography in patients with CRC was preapproved by the Institutional Review Board (IRB) at GIST (No. 20210115-BR-58-03-02). All work related to human tissues was conducted in accordance with the Helsinki Declaration. All patients were informed and signed a written informed consent prior to the study.

Cell lines and culture

The human CRC cell lines HCT116 (Cat# 10247, RRID:CVCL_0291), SW480 (Cat# 10228, RRID:CVCL_0546), LoVo (Cat# 10229, RRID:CVCL_0399), HCT15 (Cat# 10225, RRID:CVCL_0292), LS174T (Cat# 10188, RRID:CVCL_1384), and HT29 (Cat# 30038, RRID:CVCL_0320) and the human normal fibroblast cell line MCR-5 (Cat# 10171, RRID:CVCL_0440) were purchased from the Korean Cell Line Bank (KCLB, Seoul, Republic of Korea). The SW48 cell line (Cat# CCL-231, RRID:CVCL_1724) was purchased from American Type Culture Collection (ATCC, Rockville, MD, USA). The normal colon cell line NCM460D (Cat# NCM460D, RRID:CVCL_IS47) was purchased from INCELL (San Antonio, TX, USA). All cell lines were cultured according to the supplier's instructions. Additionally, we used the dysadherin KO SW480 cell line, OE HCT116 cell line, KD MDA-MB-231 cell line and OE PLC/PRF/5 cell line that were established in previous studies[24,27,54]. The cells were routinely tested for mycoplasma contamination every 6 months using the e-MycoTM Mycoplasma detection kit (iNtron Biotechnology, Seongnam, Republic of Korea, Cat# 25235), and all experiments were performed within 20 passages from the first thaw.

Bioinformatic assessment

GSEA was performed as described in our previous study[24]. Briefly, a DEG list was obtained from the Gene Expression Omnibus database using the GSE21510 dataset by comparing two groups of CRC patients, which were divided according to the median value of dysadherin expression level ($n = 52$/group). The total DEG lists ($p < 0.001$) were applied as a ranked gene list. GSEA of the ranked gene list was performed using the Java implementation of GSEA obtained from http://www.broadinstitue.org/gsea/ (1000 permutations; minimum term size: 15; maximum term size: 500; C2: all curated genes). The normalized enrichment score accounts for the differences in gene set size and the false discovery rate (q-value) was used to set a significance threshold.

For the analysis of scRNA-seq data, we reanalyzed the GSE144735 and GSE225857 datasets using Seurat for normalization; identified variable features; and performed scaling, clustering, and uniform manifold approximation and projection (UMAP) generation with default parameters. Cell type annotations were imported from the original dataset. In GSE144735, epithelial cells were classified as normal tissue or tumor tissue. In GSE225857, cancer cells were classified as dysadherin-expressing or -nonexpressing cells. We used the Enrichr web server (https://maayanlab.cloud/Enrichr/) to classify the genes based on the Reactome 2023 ontology. For the trajectory analysis, Monocle 3 was used to infer the cell differentiation trajectories. These algorithms place the cells along a trajectory corresponding to a biological process (in our case, cell differentiation) by taking advantage of an individual cell's asynchronous progression under an unsupervised framework. For the analysis of the spatial transcriptome, we reanalyzed the GSE226997 dataset using Seurat to normalize and scale all gene expression.

RNA sequencing was performed to determine the difference in gene expression signatures between dysadherin KO and WT SW480 cells in a previous study[24], and between dysadherin OE and EV HCT116 cells. Briefly, an mRNA sequencing library was prepared using the TruSeq Stranded mRNA Sample Preparation Kit and the Illumina NextSeq platform. The list of DEGs ($n = 4437$, $p < 0.05$) altered in dysadherin KO SW480 cells was subjected to IPA (Qiagen, Redwood City, CA, USA) to identify the canonical pathways that were significantly associated with dysadherin KO. Furthermore, the list of DEGs ($n = 4453$, $p < 0.01$, Supplementary Data 3) altered in dysadherin OE HCT116 cells was subjected to EnrichR to identify the gene signatures that were significantly associated with dysadherin OE.

Fxyd5 knockout mice

Fxyd5$^{-/-}$ mice were generated in a previous study[24]. Briefly, *Fxyd5*$^{-/-}$ mice were generated using CRISPR/Cas9 technology. Three guide RNAs (gRNA sequences: AGGCTGCTAGGCATCTCGGGGGG, TCTTCCTGGGCTCGGTCACGTGG, and CCCCGATGAGCGATACAGAGACA) were used to cut the genomic DNA at *Fxyd5* introns 1 and 7, resulting in the deletion of exons 2-7, which contain the ATG start codon and most of the coding sequence. *Fxyd5*$^{-/-}$ mice were purchased from Vitalstar (Beijing, China).

Animal studies

Mice were housed in temperature-controlled pathogen-free conditions (around 24 °C, 50% humidity) under a 12 h light/dark cycle. A splenic injection experiment was performed to evaluate the steps governing metastasis and distant organ colonization. Pain and distress were monitored by observing the weight loss exceeding 20% of body weight, hunched posture, lethargy, lack of movement, and rapid growth of tumor masses as permitted by the IACUC of GIST. Mice exhibiting any of these signs were sacrificed. For this model, cell lines were tagged with luciferase (pCMV-luc). The cells were inoculated into the spleens of 8 weeks old male NSG mice (NOD.Cg-Prkdc^{scid} Il2rg^{tm1Wjl}/SzJ, Cat#005557; Jackson Laboratory, Bar Harbor, ME, USA) followed by splenectomy (1×10^6 cells/mouse); the surviving cells that grew in distant organs then contributed to the formation of liver metastases. Liver metastasis was routinely monitored weekly by visualizing luciferase activity for 21 days using the IVIS Lumina III in vivo Imaging System (Perkin Elmer, Waltham, Massachusetts, US). After the mice were sacrificed, the liver was removed to determine liver metastasis.

To establish humanized mice, NSG Tg(CMV-IL-3, CSF2, KITLG)1Eav/MloySzJ (SGM3, Cat#013062) mice were purchased from Jackson Laboratory. We used female mice because engraftment of CD34$^+$ cells is more efficient in female mice. Mice were 4 weeks old at the time of transplantation. Busulfan (Sigma–Aldrich, St. Louis, MO, USA, Cat# B2635) was dissolved in dimethyl sulfoxide (Sigma–Aldrich, Cat# D2650) and diluted with PBS. The liquid busulfan solution was intraperitoneally injected into NSG-SGM3 mice (25 mg/kg body weight) 48 and 24 h prior to transplantation of human CD34$^+$ cells (Lonza, Slough, Berkshire, UK, Cat# 2C-101). The next day, 1×10^5 human CD34$^+$ cells in 100 µL of PBS were transplanted into NSG-SGM3 mice via intravenous injection. Eight weeks after transplantation, human cell reconstitution was assessed by flow cytometry. Blood samples were collected via the retro-orbital plexus with a heparinized capillary tube. The antibodies anti-human CD45-APC and anti-mouse CD45-PE were added, and whole blood was incubated in the dark at room temperature for 20 min. Red blood cells were lysed using RBC lysis buffer (Sigma-Aldrich, Cat# R7757). Flow cytometry analysis was performed using BD Accuri™ C6 (Becton Dickinson, Sunnyvale, CA, USA). Fluorescence-activated cell sorting data were analyzed using FlowJo software (Treestar Inc., Ashland, OR, USA).

Histological assessment

For clinical analysis, tissues from 50 patients with colon cancer and 10 patients with carcinoma in situ were embedded in optimal cutting temperature (OCT) compound (Leica, Wetzlar, Germany, Cat#3801480), cut at 10 µm with a cryostat (HM525 NX, Thermo Fisher

Scientific, Waltham, MA, USA) and immunostained by IF to detect target molecules using the primary antibodies described in Table S3. The biospecimens and data used for this study were provided by the Biobank of Chonnam National University Hwasun Hospital, a member of the Korea Biobank Network.

To analyze the liver metastasis mouse model, all liver tissue samples were embedded in OCT compound, cut at 10 μm with a cryostat, immunostained, and visualized by IF. To measure the metastatic burden at the microscopic level and histologically observe the morphology of the tissues, cryosections were stained with hematoxylin (Dako, Carpinteria, CA, USA, Cat# S3309) and eosin (Millipore, Billerica, MA, USA, Cat# 1.02439.0500) according to the supplier's instructions.

In both clinical and mouse tissues, target proteins were visualized by IF using specific antibodies and secondary antibodies conjugated with fluorescent dyes. Nuclei were counterstained with 4′,6-diamidino-2-phenylindole (DAPI, Sigma–Aldrich, Cat# D9542). Fluorescence signals were visualized using an Axio Imager 2 (Carl Zeiss, Oberkochen, Germany) at a total magnification of 100x or 200x. The relative expression levels of the proteins were assessed based on the fluorescence intensity and were normalized to the intensity of DAPI. The antibodies used are listed in Table S3.

Clinical analysis

123 patients with CRC were immunostained to detect dysadherin and MMP9. The slides contained 3 tumor tissue cores and 2 matched normal tissue cores from each patient. After heat-induced epitope retrieval, the slides were permeabilized and incubated with primary antibodies (1:500) at 4 °C overnight. Following repeated washing steps, the slides were incubated with secondary antibodies (1:1000) for 30 min at room temperature. Nuclei were counterstained with DAPI. Fluorescence signals were visualized using an Axio Imager 2 (Carl Zeiss) at a total magnification of 100x or 200x. The relative expression levels of the target proteins were measured based on the fluorescence intensity as described above and were normalized to the DAPI intensity. The ratio of dysadherin or MMP9 expression in tumor tissues versus normal tissues (average intensity of 3 tumor tissue cores/average intensity of 2 normal tissue cores) was used to determine the association of dysadherin or MMP9 expression with clinicopathological variables. Patients were divided into two group according to median value; high ($n = 62$) and low ($n = 61$). Recurrence-free survival (RFS) was defined as the time from the date of surgery to the date of recurrence or death, whichever occurred first, and patients who were alive at the last follow-up were recorded at that time If neither event had occurred at the time of analysis, the patient was censored. Overall survival (OS) was calculated from the diagnosis of disease to death from any cause, and patients who were alive at last follow-up were recorded at that time. Survival was calculated using the Kaplan-Meier method, and comparisons were made using log-rank tests. Statistical analyses were performed using GraphPad Prism 9.0 (GraphPad Software, Inc., San Diego, CA, USA).

In situ zymography

The localized proteolytic activity was determined by using DQ-collagen I or DQ-gelatin (Invitrogen, Carlsbad, MA, USA, Cat# D12060, D12054) as a substrate. In unfixed cryosections of tissue, frozen sections were thawed for 5 min and washed with PBS twice for 5 min each to remove OCT compound. This was followed by the pre-incubation of the sections in MMP activation buffer (50 mM Tris-HCl pH 7.5, 150 mM NaCl, 5 mM $CaCl_2$, and 0.2 mM sodium azide) in an incubation chamber at 37 °C. The sections were then incubated overnight at 37 °C with DQ-collagen I or DQ-gelatin (1 mg/mL diluted 1:50 in activation buffer), followed by three washes with PBS. The sections were then fixed with 4% paraformaldehyde for 10 min and stained for other markers and DAPI. Sections were imaged using an Axio Imager 2 (Carl Zeiss).

Gel zymography

Gelatinolytic activities in the culture media were evaluated via gelatin zymography. Gelatin-containing gels were prepared in the laboratory by adding 2 mL of 4 mg/mL gelatin solution from calf skin (Sigma-Aldrich, Cat# G9382) to 10 mL of 10% acrylamide gel. The supernatant samples (25 μL) were mixed with equal volumes of 5X zymography sample buffer (125 mM Tris-HCl (pH 6.8), 20% glycerol, 4% SDS, and 0.01% bromophenol blue), loaded onto polyacrylamide gels containing gelatin under nonreducing conditions, and electrophoresed in 2.5 mM Tris-HCl, 19.2 mM glycine, and 0.01% SDS (pH 8.3) at 100 V. After electrophoresis, the gels were washed twice for 30 min in enzyme renaturing buffer (5 mM $CaCl_2$, 1 μM $ZnCl_2$, 2.5% (v/v) Triton X-100, and 50 mM Tris-HCl (pH 7.5)) and incubated overnight in zymogram development buffer (5 mM $CaCl_2$, 1 μM $ZnCl_2$, 1% (v/v) Triton X-100, and 50 mM Tris-HCl (pH 7.5)). The gels were then stained with Coomassie blue R-250 and destained with 40% methanol and 10% acetic acid. Areas of MMP activity appeared as clear bands.

Apc$^{Min/+}$ mouse tumor-derived organoid culture

Single cells were isolated from the intestinal tumors of 24-week-old *Apc*$^{Min/+}$;*Fxyd5*$^{+/+}$ and *Apc*$^{Min/+}$;*Fxyd5*$^{-/-}$ mice and cultured as described in a previous report with slight modifications[24]. Briefly, mouse intestines containing tumors were incubated with ethylenediaminetetraacetic acid (EDTA) chelation buffer (EDTA 3 mM, Dithiothreitol 50 μM in PBS) for 60 min on ice. After chelation, the detached normal intestinal epithelial cells were removed by centrifugation; tumor cells remained attached to the mesenchyme. Intestinal fragments with tumor cells were then dissociated with collagenase as described in the previous report. The isolated tumor cells were counted and pelleted, and a total of 2000 cells were seeded in 96-well plates or mixed with 10 μL of Matrigel (Corning Matrigel® Growth Factor Reduced Basement Membrane Matrix, Cat# 356231, Corning, NY, USA). After the polymerization of Matrigel, 200 μL of IntestiCult™ Organoid Growth Medium (Mouse, Cat# 06005, STEMCELL Technology) was added. Using tumoroid, we performed the zymography, so we mixed the DQ-collagen I in Matrigel when seeding the tumoroid.

Small interfering RNA-mediated KD and establishment of inducible MMP9 KD cells

Dysadherin, MMP9, c-JUN and MAZ siRNAs and a nonspecific negative control siRNA (Bioneer, Daejeon, Republic of Korea) were used to generate knockdown cells. Cells were transfected with siRNA or control siRNA in media (serum-, phenol-, or antibiotic-free) with Lipofectamine™ 2000 (Invitrogen, Cat# 11668019) according to the manufacturer's instructions. To establish the inducible MMP9 KD cell line, the most effective siRNA sequence was synthesized as a short hairpin RNA (shRNA) and inserted into a lentiviral Tet-pLKO-puro vector (Addgene, Cambridge, MA, USA, Cat# 21915). The shRNA vector was then transfected into 293FT cells (Invitrogen, Cat# R70007) with a viral packaging mixture (Sigma–Aldrich, Cat# SHP001), and the viral mixture was used for transfection. Puromycin (Sigma–Aldrich, Cat# P9620) was used as the selection marker. The knockdown efficiency was confirmed on the basis of the relative expression of mRNA, which was detected via real-time polymerase chain reaction (RT–qPCR). The siRNA sequences are listed in Table S4.

Establishing MMP9-overexpressing cell lines

To establish the MMP9 OE cell line, WT and dysadherin KO SW480 cells were transfected with an MMP9 expression vector (pCMV-MMP9, Sino Biological Inc. Beijing, China, Cat# HG10327-UT) and selected with hygromycin B for 1 week. Dilution cloning was performed, and the

overexpression of the MMP9 gene was confirmed by RT–qPCR and immunoblot analysis.

RNA isolation and real-time qPCR

Total RNA was isolated using RNAiso reagent (Takara, Shiga, Japan, Cat# 9108). The RNA purity was verified by measuring the 260/280 and 260/230 absorbance ratios. cDNA were synthesized from 0.5 μg of total RNA using the PrimeScript™ 1st strand cDNA Synthesis Kit (Takara Biomedicals, Kusatsu, Japan, Cat# 6110 A) with random primers. qPCR was performed using Power SYBR Green PCR Master Mix (Applied Biosystems, Foster City, CA, USA, Cat# 10187094) and StepOne Real-time PCR systems (Applied Biosystems). The primers used are listed in Supplementary Data 4.

Protein isolation and immunoblot analysis

Tissues or cells were homogenized in RIPA buffer for 20 min on ice. A BCA assay kit was used to determine protein concentrations using a bicinchoninic acid (BCA) assay (Thermo Fisher Scientific, Cat# A55860). The proteins were denatured with SDS (T&I, Gangwon, Republic of Korea, Cat# BSS-9005) thereby boiling at 95 °C for 5 min. 10 μg of total protein were separated via 10% polyacrylamide gel electrophoresis, and the separated proteins were transferred to a polyvinylidene difluoride membrane (Millipore, Cat# 10600021). The membranes were blocked with 10% bovine serum albumin (BOVOGEN, Keilor East, Australia, Cat# BSAS 0.1) and incubated overnight at 4 °C with the primary antibodies. The membranes were then treated with secondary antibodies conjugated to horseradish peroxidase (HRP) with incubating on room temperature. Chemiluminescence of HRP was developed with Super Signal West Dura Extended Duration Substrate (Thermo Fisher Scientific, Cat# 34075) and detected with a Digital 8 Imaging System (ProteinSimple, 3040 Oakmead Village Drive, Santa Clara). The numbers under each image are fold changes in band intensity relative to the initial condition, determined using Image J. The antibodies used for immunoblot analyses are listed in Table S3.

Chromatin immunoprecipitation assay

An Ez ChIP kit (Millipore, Cat# 17-371) was used according to the manufacturer's instructions. For ChIP assays, 6×10^6 cells in culture were fixed in 1% formaldehyde to crosslink DNA to bound proteins, and the reaction was quenched by the addition of 0.125 M glycine. The cells were washed with PBS and collected at 4 °C in the presence of protease inhibitor cocktail (Sigma-Aldrich, Cat# S8830). The collected cells were resuspended in 500 μL of ChIP sonication buffer (20% SDS and protease inhibitors), followed by sonication and centrifugation of the fragments (200–700 bp long) at 2000 × *g*. The fragmented chromatin in the supernatant was immunoprecipitated using an anti-c-JUN antibody at 4 °C overnight. Protein A agarose beads were added to the samples containing chromatin-antibody complexes, which were subsequently centrifuged to sediment the beads. The beads were washed with cold buffer, and the DNA was eluted with elution buffer. DNA in the supernatant was precipitated using a high-salt method according to the manufacturer's instructions. The extracted DNA was subjected to PCR amplification with specific primers designed around the c-JUN binding site of the MMP9 promoter.

Luciferase reporter assay

A luciferase reporter assay reflecting MMP9 transcription was performed using a MMP9 promoter region (−1317 to +20)-containing vector (GeneCopoeia, Maryland, USA, Cat# HPRM45843). A mixture of vector, β-galactosidase, and Lipofectamine was made at a ratio of 1 μg:1 μg:2 μL in 300 μL of OptiMEM medium/well. After the cells were transfected with the vector, they were treated with MK-0429, PND-1186 or T-5224 (MedChemExpress, Monmouth Junction, NJ, USA, Cat# HY-15102, HY-13917, HY-12270). Cell lysis buffer was added after 24 h of treatment. To measure luciferase activity, a Renilla luciferase assay system (Promega, Madison, WI, USA, Cat# E2810) was used, and activity was measured by a SpectraMax L (Molecular Devices, San Jose, CA, USA) according to the manufacturer's instructions. Relative luciferase activity was normalized to that of β-galactosidase.

3D invasion assay

To form spheroids, cells were seeded under sphere culture conditions (poly-HEMA-coated plates; Sigma-Aldrich Cat# P3932) for 4 days. The spheroids were embedded in 2.0 mg/mL Matrigel (Corning) in a 24-well plate and allowed to invade for up to 72 h at 37 °C. Images were taken using a phase-contrast microscope (Carl Zeiss, biological triplicates).

Anchorage-independent growth assay

Agar (0.35%, 1 mL) in culture media was added to the bottom layer of each well in a 12-well plate. For the top layer in each well, 1×10^3 cells were resuspended in 1 mL of a mixture comprising 0.2% agar and RPMI 1640 media. The cells were incubated at 37 °C in 5% CO_2 for 2 weeks, after which the colonies were stained with crystal violet, photographed by inverted phase-contrast microscopy (Leica), and counted using ImagePro premier 9 (Image-Pro Premier 9.0, Media Cybernetics, MD, USA).

Conditioned media preparation

CRC cells (5×10^5) were seeded in 6-well plates. After 24 h, the media was changed to serum-free media and incubated for 24 h. The media was subsequently collected and filtered through a 0.4-micron filter. The CM was stored at −20 °C until use.

Enzyme-linked immunosorbent assay

CM from each group was collected and stored at −80 °C before ELISAs. The concentration of total TGF-β1 was measured using a LEGEND MAX Free Total TGF-β1 ELISA Kit (BioLegend, San Diego, CA, USA, Cat# 436707), while the concentration of the active form of TGF-β1 was measured using a LEGEND MAX Free Active TGF-β1 ELISA Kit (BioLegend, Cat# 437707) according to the manufacturer's instructions.

IFN-γ and IL-4 levels were detected and quantified in tumor tissue from a humanized mouse model using an IFN-γ ELISA kit and an IL-4 ELISA kit (Invitrogen, Cat# KHC4021, KHC0041). ELISAs were performed according to the manufacturer's instructions. The absorbance was read at a wavelength of 450 nm using a microplate reader (BioTek, Winooski, VT, USA).

Statistics and reproducibility

No statistical methods were used to predetermine sample sizes but our sample sizes are similar to those reported in previous studies. In vitro experiments were all performed on at least three separate occasions and in vivo experiments were performed on five or six separate occasions. All the results are expressed as the mean ± standard error of the mean. Statistical comparisons of data from 2 groups were carried out by Student's *t* test or two-way ANOVA with the Bonferroni multiple comparison test, and statistical comparisons of 3 or more groups were carried out by one-way ANOVA with Dunnett's multiple comparison test using GraphPad Prism (GraphPad Software, Inc., San Diego, CA, USA). The specific numbers of biological replicates used are provided in the figure legends. Asterisks indicate statistical significance. *, **, and *** indicate $p < 0.05$, <0.01, and <0.001, respectively.

Reporting summary

Further information on research design is available in the Nature Portfolio Reporting Summary linked to this article.

Data availability

The data that support the findings of this study are available in the main figures and the supplementary material of this article. The

analyzed RNA-sequencing data are available in Supplementary Information. The raw sequencing data used in this study are available in the Gene Expression Omnibus (GEO, https://www.ncbi.nlm.nih.gov/geo/) under accession number GSE21510, GSE144735, GSE225857, GSE14333, GSE17538 and GSE73255. Source data are provided with this paper.

References

1. Rahimi Pordanjani, S., Baeradeh, N., Lotfi, M. H. & Pourmohammadi, B. Epidemiology of colorectal cancer: incidence, mortality, survival rates and risk factors. *Razi J. Med. Sci.* **23**, 41–50 (2016).
2. Sung, H. et al. Global cancer statistics 2020: GLOBOCAN estimates of incidence and mortality worldwide for 36 cancers in 185 countries. *CA: Cancer J. Clinicians* **71**, 209–249 (2021).
3. Vatandoust, S., Price, T. J. & Karapetis, C. S. Colorectal cancer: Metastases to a single organ. *World J. Gastroenterol.* **21**, 11767 (2015).
4. Baghban, R. et al. Tumor microenvironment complexity and therapeutic implications at a glance. *Cell Commun. Signal.* **18**, 1–19 (2020).
5. Jahanban-Esfahlan, R. et al. RGD delivery of truncated coagulase to tumor vasculature affords local thrombotic activity to induce infarction of tumors in mice. *Sci. Rep.* **7**, 8126 (2017).
6. Poltavets, V., Kochetkova, M., Pitson, S. M. & Samuel, M. S. The role of the extracellular matrix and its molecular and cellular regulators in cancer cell plasticity. *Front. Oncol.* **8**, 431 (2018).
7. Yuan, Z. et al. Extracellular matrix remodeling in tumor progression and immune escape: from mechanisms to treatments. *Mol. cancer* **22**, 48 (2023).
8. Quail, D. F. & Joyce, J. A. Microenvironmental regulation of tumor progression and metastasis. *Nat. Med.* **19**, 1423–1437 (2013).
9. Zafari, N. et al. The role of the tumor microenvironment in colorectal cancer and the potential therapeutic approaches. *J. Clin. Lab. Anal.* **36**, e24585 (2022).
10. Hynes, R. O. The extracellular matrix: not just pretty fibrils. *Science* **326**, 1216–1219 (2009).
11. Cox, T. R. The matrix in cancer. *Nat. Rev. Cancer* **21**, 217–238 (2021).
12. Kalluri, R. The biology and function of fibroblasts in cancer. *Nat. Rev. Cancer* **16**, 582–598 (2016).
13. Barbazán, J. & Vignjevic, D. M. Cancer associated fibroblasts: is the force the path to the dark side? *Curr. Opin. cell Biol.* **56**, 71–79 (2019).
14. Heneberg, P. Paracrine tumor signaling induces transdifferentiation of surrounding fibroblasts. *Crit. Rev. Oncol./Hematol.* **97**, 303–311 (2016).
15. Ishii, G., Ochiai, A. & Neri, S. Phenotypic and functional heterogeneity of cancer-associated fibroblast within the tumor microenvironment. *Adv. Drug Deliv. Rev.* **99**, 186–196 (2016).
16. Orimo, A. et al. Stromal fibroblasts present in invasive human breast carcinomas promote tumor growth and angiogenesis through elevated SDF-1/CXCL12 secretion. *Cell* **121**, 335–348 (2005).
17. Gilkes, D. M., Bajpai, S., Chaturvedi, P., Wirtz, D. & Semenza, G. L. Hypoxia-inducible factor 1 (HIF-1) promotes extracellular matrix remodeling under hypoxic conditions by inducing P4HA1, P4HA2, and PLOD2 expression in fibroblasts. *J. Biol. Chem.* **288**, 10819–10829 (2013).
18. Erler, J. T. et al. Lysyl oxidase is essential for hypoxia-induced metastasis. *Nature* **440**, 1222–1226 (2006).
19. Winkler, J., Abisoye-Ogunniyan, A., Metcalf, K. J. & Werb, Z. Concepts of extracellular matrix remodelling in tumour progression and metastasis. *Nat. Commun.* **11**, 5120 (2020).
20. Erdogan, B. & Webb, D. J. Cancer-associated fibroblasts modulate growth factor signaling and extracellular matrix remodeling to regulate tumor metastasis. *Biochem. Soc. Trans.* **45**, 229–236 (2017).
21. Cox, T. R. & Erler, J. T. Remodeling and homeostasis of the extracellular matrix: implications for fibrotic diseases and cancer. *Dis. Models Mechanisms* **4**, 165–178 (2011).
22. Ino, Y., Gotoh, M., Sakamoto, M., Tsukagoshi, K. & Hirohashi, S. Dysadherin, a cancer-associated cell membrane glycoprotein, down-regulates E-cadherin and promotes metastasis. *Proc. Natl. Acad. Sci.* **99**, 365–370 (2002).
23. Shimada, Y. et al. Clinical significance of dysadherin expression in gastric cancer patients. *Clin. Cancer Res.* **10**, 2818–2823 (2004).
24. Park, S.-Y. et al. Dysadherin awakens mechanical forces and promotes colorectal cancer progression. *Theranostics* **12**, 4399 (2022).
25. Aoki, S. et al. Prognostic significance of dysadherin expression in advanced colorectal carcinoma. *Br. J. Cancer* **88**, 726–732 (2003).
26. Shimamura, T. et al. Dysadherin expression facilitates cell motility and metastatic potential of human pancreatic cancer cells. *Cancer Res.* **64**, 6989–6995 (2004).
27. Lee, Y. K. et al. Dysadherin expression promotes the motility and survival of human breast cancer cells by AKT activation. *Cancer Sci.* **103**, 1280–1289 (2012).
28. Cooper, J. & Giancotti, F. G. Integrin signaling in cancer: mechanotransduction, stemness, epithelial plasticity, and therapeutic resistance. *Cancer cell* **35**, 347–367 (2019).
29. Lamouille, S., Xu, J. & Derynck, R. Molecular mechanisms of epithelial–mesenchymal transition. *Nat. Rev. Mol. cell Biol.* **15**, 178–196 (2014).
30. Afshar K., Sanaei M. J., Ravari M. S., Pourbagheri-Sigaroodi A. & Bashash D. An overview of extracellular matrix and its remodeling in the development of cancer and metastasis with a glance at therapeutic approaches. *Cell Biochem. Funct.* **41**, 930–952 (2023).
31. Pickup, M. W., Mouw, J. K. & Weaver, V. M. The extracellular matrix modulates the hallmarks of cancer. *EMBO Rep.* **15**, 1243–1253 (2014).
32. O'Connor, R. S. et al. Substrate rigidity regulates human T cell activation and proliferation. *J. Immunol.* **189**, 1330–1339 (2012).
33. Meyaard, L. The inhibitory collagen receptor LAIR-1 (CD305). *J. Leucoc. Biol.* **83**, 799–803 (2008).
34. Patel N. R. et al. Cell elasticity determines macrophage function. *PLoS One* **7**, e41024 (2012).
35. Li, H., Qiu, Z., Li, F. & Wang, C. The relationship between MMP-2 and MMP-9 expression levels with breast cancer incidence and prognosis. *Oncol. Lett.* **14**, 5865–5870 (2017).
36. Griffith, B. G. et al. FAK regulates IL-33 expression by controlling chromatin accessibility at c-Jun motifs. *Sci. Rep.* **11**, 229 (2021).
37. Bauvois, B. New facets of matrix metalloproteinases MMP-2 and MMP-9 as cell surface transducers: outside-in signaling and relationship to tumor progression. *Biochimica et. Biophysica Acta (BBA)-Rev. Cancer* **1825**, 29–36 (2012).
38. Ma, J. et al. Expression of RSK4, CD44 and MMP-9 is upregulated and positively correlated in metastatic ccRCC. *Diagnostic Pathol.* **15**, 1–10 (2020).
39. Fridman, R., Toth, M., Chvyrkova, I., Meroueh, S. O. & Mobashery, S. Cell surface association of matrix metalloproteinase-9 (gelatinase B). *Cancer Metastasis Rev.* **22**, 153–166 (2003).
40. Dayer, C. & Stamenkovic, I. Recruitment of matrix metalloproteinase-9 (MMP-9) to the fibroblast cell surface by lysyl hydroxylase 3 (LH3) triggers transforming growth factor-β (TGF-β) activation and fibroblast differentiation. *J. Biol. Chem.* **290**, 13763–13778 (2015).
41. Wang, L. et al. Hot and cold tumors: Immunological features and the therapeutic strategies. *MedComm* **4**, e343 (2023).
42. Luo, F. et al. The BCL-2 inhibitor APG-2575 resets tumor-associated macrophages toward the M1 phenotype, promoting a favorable

response to anti-PD-1 therapy via NLRP3 activation. *Cell. Mol. Immunol.* **21**, 60–79 (2024).
43. Ma, Y. et al. Remodeling the tumor-immune microenvironment by anti-CTLA4 blockade enhanced subsequent anti-PD-1 efficacy in advanced nasopharyngeal carcinoma. *NPJ Precis. Oncol.* **8**, 65 (2024).
44. Jiang, X. et al. Role of the tumor microenvironment in PD-L1/PD-1-mediated tumor immune escape. *Mol.Cancer* **18**, 1–17 (2019).
45. Zhang, A., Miao, K., Sun, H. & Deng, C.-X. Tumor heterogeneity reshapes the tumor microenvironment to influence drug resistance. *Int. J. Biol. Sci.* **18**, 3019 (2022).
46. Fidler, I. J. & Kripke, M. L. Metastasis results from preexisting variant cells within a malignant tumor. *Science* **197**, 893–895 (1977).
47. Studebaker, A. W. et al. Fibroblasts isolated from common sites of breast cancer metastasis enhance cancer cell growth rates and invasiveness in an interleukin-6–dependent manner. *Cancer Res.* **68**, 9087–9095 (2008).
48. Ding, X. et al. HGF-mediated crosstalk between cancer-associated fibroblasts and MET-unamplified gastric cancer cells activates coordinated tumorigenesis and metastasis. *Cell death Dis.* **9**, 867 (2018).
49. Kim, S. J. et al. Expression of interleukin-8 correlates with angiogenesis, tumorigenicity, and metastasis of human prostate cancer cells implanted orthotopically in nude mice. *Neoplasia* **3**, 33–42 (2001).
50. O'Brien, M., Ernst, M. & Poh, A. R. An intrasplenic injection model of pancreatic cancer metastasis to the liver in mice. *STAR Protoc.* **4**, 102021 (2023).
51. Gómez-Cuadrado, L., Tracey, N., Ma, R., Qian, B. & Brunton, V. G. Mouse models of metastasis: progress and prospects. *Dis. Models Mechanisms* **10**, 1061–1074 (2017).
52. Nam, J.-S. et al. Chemokine (CC motif) ligand 2 mediates the prometastatic effect of dysadherin in human breast cancer cells. *Cancer Res.* **66**, 7176–7184 (2006).
53. Nam, J.-S., Hirohashi, S. & Wakefield, L. M. Dysadherin: a new player in cancer progression. *Cancer Lett.* **255**, 161–169 (2007).
54. Park, J.-R. et al. Dysadherin can enhance tumorigenesis by conferring properties of stem-like cells to hepatocellular carcinoma cells. *J. Hepatol.* **54**, 122–131 (2011).

Acknowledgements

J-S Nam was supported by the National Research Foundation of Korea (NRF) grant funded by the Korean government (MSIT) (RS-2023-NR077237, RS-2024-00411137, RS-2024-00441157) and by CNUH-GIST research Collaboration grant funded by the Gwangju Institute of Science and Technology (GIST) in 2024. The anti-dysadherin monoclonal antibody (M53) was kindly gifted by Dr. Yoshinori Ino (National Cancer Center Research Institute, Tokyo, Japan). This manuscript was edited for proper English language, grammar, punctuation, spelling, and overall style by the highly qualified native English-speaking editors at American Journal Experts (Durham, NC, USA). We thank Dr. Melissa Stauffer (Scientific Editing Solutions, Walworth, WI, USA) for critical reading of the manuscript.

Author contributions

C-J Lee: conceptualization, data curation, investigation, visualization, writing-original draft, and writing-review and editing; T-Y Jang, S-E Jeon, H-J Yun, Y-H Cho, D-Y Lim: investigation and validation; J-S Nam: conceptualization, resources, supervision, funding acquisition, validation, methodology, project administration, and writing-review and editing.

Competing interests

The authors declare no competing interests.

Additional information

Supplementary information The online version contains supplementary material available at https://doi.org/10.1038/s41467-024-54920-9.

Correspondence and requests for materials should be addressed to Jeong-Seok Nam.

Peer review information *Nature Communications* thanks Achilleas Theocharis and the other anonymous reviewer(s) for their contribution to the peer review of this work. A peer review file is available.